Supplementary information

Structural and Optical Properties of $Cs_2AgBiBr_6$ Double Perovskite.

Laura Schade,[1] Adam D. Wright,[1] Roger D. Johnson,[1] Markus Dollmann,[1] Bernard Wenger[1], Pabitra K. Nayak,[1] Dharmalingam Prabhakaran,[1] Laura M. Herz,[1] Robin Nicholas,[1] Henry J. Snaith,[1] and Paolo G. Radaelli[1]

Clarendon Laboratory, Department of Physics, University of Oxford, OX1 3PU, United Kingdom.

1) Characterization

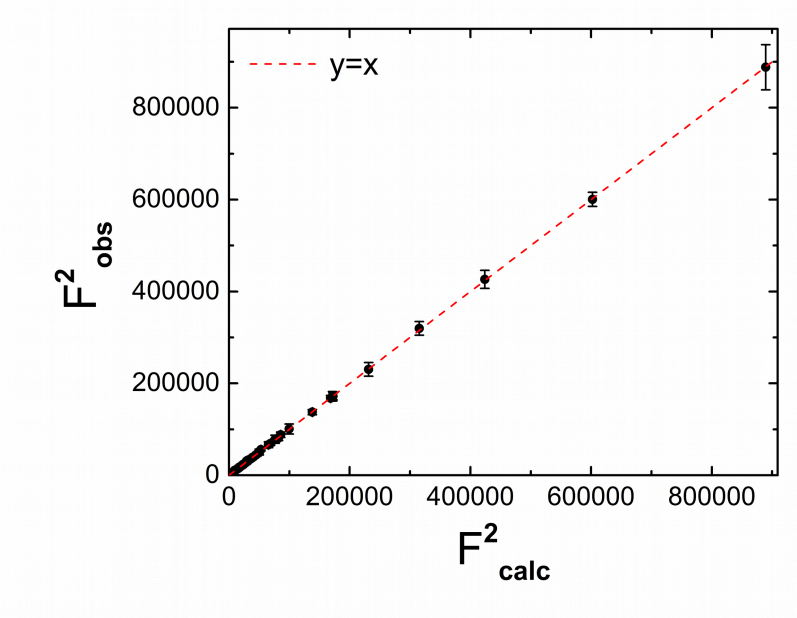

Figure S1. Plot of F^2_{calc} versus F^2_{obs} for the structural refinement of a $Cs_2AgBiBr_6$ single crystal. The red line is a guide to the eye. The data points perfectly follow the line, indicating excellent crystal quality.

Cell parameters			
Space group:	$Fm\bar{3}m$		
Z = 4			
a	11.2741(2)		
$V_{f.u.}$	358.250(1)		

Refinable atomic fractional coordinates			
Atom	*x*	*y*	*Z*
Br	0.25093(2)	-	-

Anisotropic atomic displacement parameters (x100 [Å²])			
Atom	U_{11}	U_{22}	U_{33}
Cs	4.86(1)	4.86(1)	4.86(1)
Bi	1.76(7)	1.76(7)	1.76(7)
Ag	2.50(2)	2.50(2)	2.50(2)
Br	1.69(1)	7.13(2)	7.13(2)

Data collection
measured reflections: 363
independent reflections: 35
Data reduction R_{int} : 5.33%
(Criterion for observed reflections: $I > 3.0\sigma(I)$)
observed reflections: 359
fitted parameters:9

Table S1 Room-temperature crystal structure of $Cs_2AgBiBr_6$, as refined from single crystal X-ray diffraction data. In $Fm\bar{3}m$ the atoms are located at the following Wyckoff positions. Cs: 8c (1/4, 1/4, 1/4) ; Bi: 4a (0, 0, 0); Ag: 4b (1/2, 1/2, 1/2); Br: 24e (x, 0, 0). Vf.u. stands for volume per formula unit. The off-diagonal anisotropic displacement parameters $U_{12}=U_{13}=U_{23}$ are =0 by symmetry.

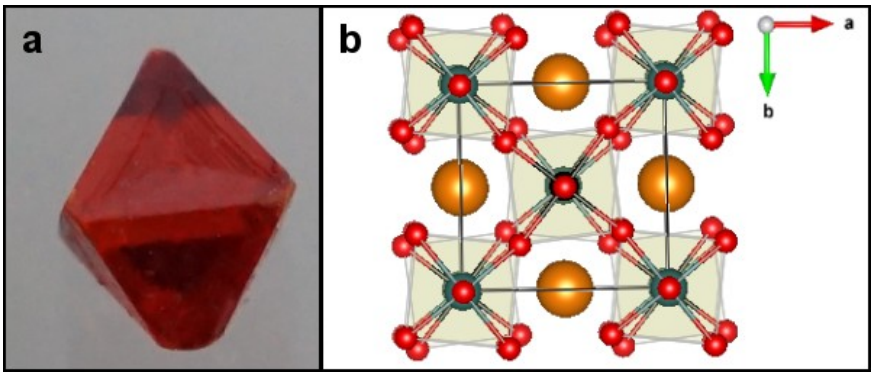

Figure S2 a) Photograph of a $Cs_2AgBiBr_6$ single crystal. b) Real-space representation of the low-temperature tetragonal crystal structure of $Cs_2AgBiBr_6$, based on our structural refinement. The orange circles represent the caesium cation, the red the bromine, and the black and grey the silver and bismuth respectively. The ochtahedra are shown in light grey for a better visualization.

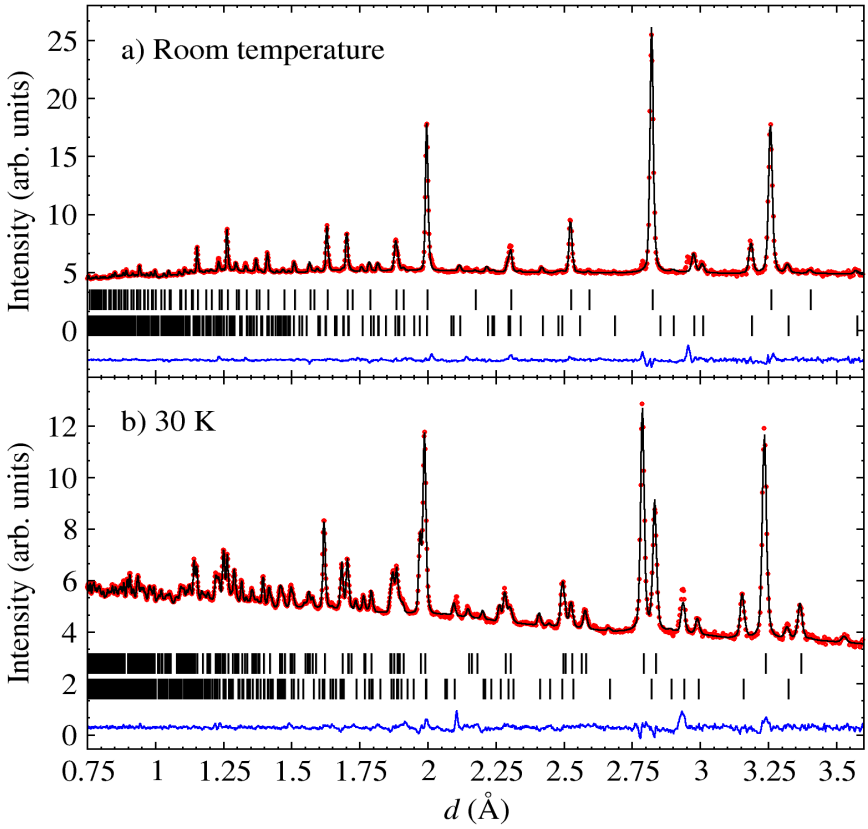

Figure S3 Neutron-diffraction patterns with Rietveld refinement for the time-of-flight neutron diffraction profiles measured for $Cs_2AgBiBr_6$ at a) room temperature and b) 30 K. The red dots represent the experimental points, while the black pattern is the calculated one. The black vertical lines represent the main phase (upper) peaks positions, and the impurities -secondary phases- (down) peaks positions.

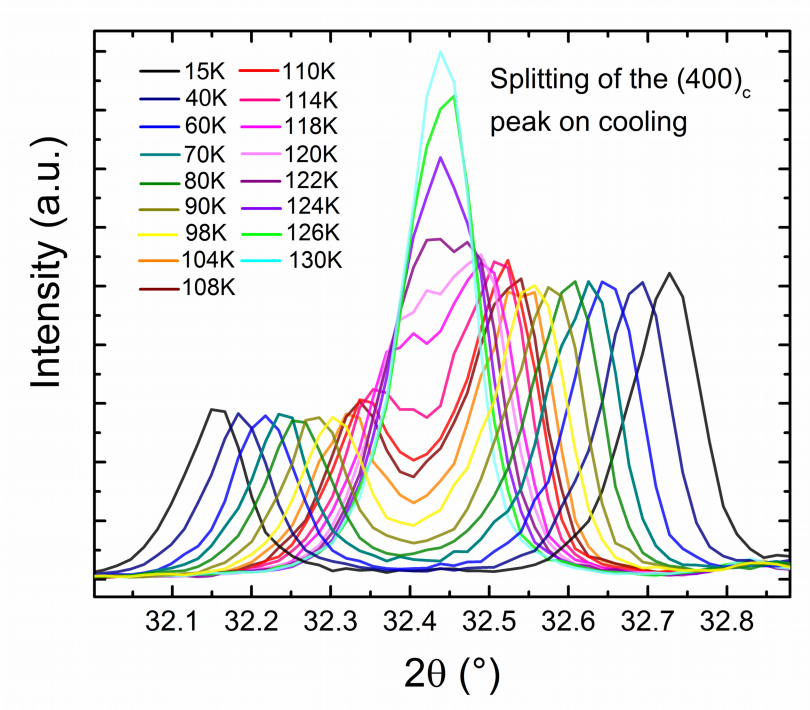

Figure S4 X-ray diffraction pattern plotted in the range ~[32-33]°, where the $(400)_c$ peak of the cubic room-temperature structure is present, in function of temperature.

Figure S4 shows the splitting of the $(400)_c$ peak of the powder X-ray diffraction pattern on cooling. We report just some of the temperatures that we collected to simplify the visualization.

2) Heat capacity – absence of hysteresis.
Figure S4 shows a detail of our capacity measurements near the structural phase transition Ts. Blue and red dots correspond to data points collected on cooling and heating, respectively. No significant thermal hysteresis was detected in these measurements.

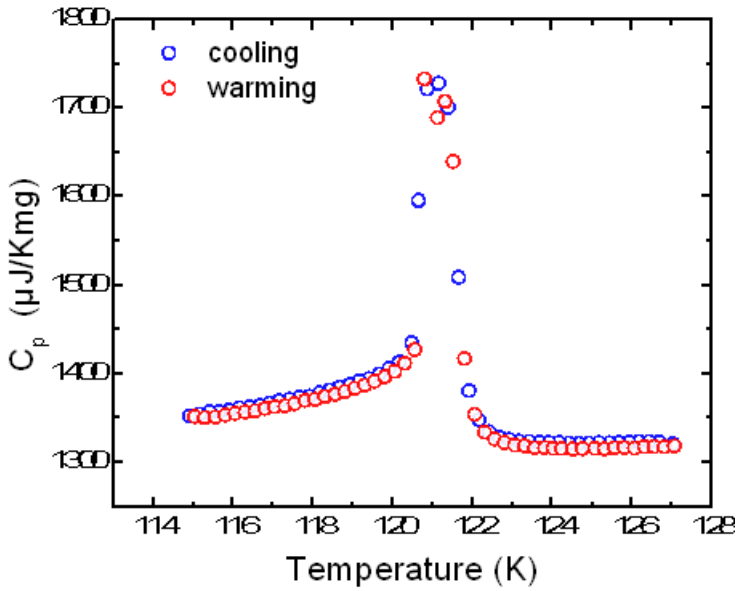

Figure S5 Specific heat capacity near the transition temperature T_s on both cooling (blue circles) and warming (red circles).

3) Modelling of the exciton transition energy.

The exciton transition energy was modelled with the following formula:

$$E_{ex} = E_{gap} - E_b = c_0 + c_1 \Delta V / V_0 + c_2 \sigma$$

where V_0 is the low-temperature unit cell volume (measured at 15 K), $\Delta V = V(T) - V(0)$, σ is the tetragonal strain defined as $\sigma = 2(a - c)/(a + c)$ and $c_0 = 2.84 \pm 0.42$ eV, $c_1 = 0.1578 \pm 0.0001$ eV and $c_2 = 1.01 \pm 0.02$ eV are fitted parameters.

4) Room temperature photoluminescence

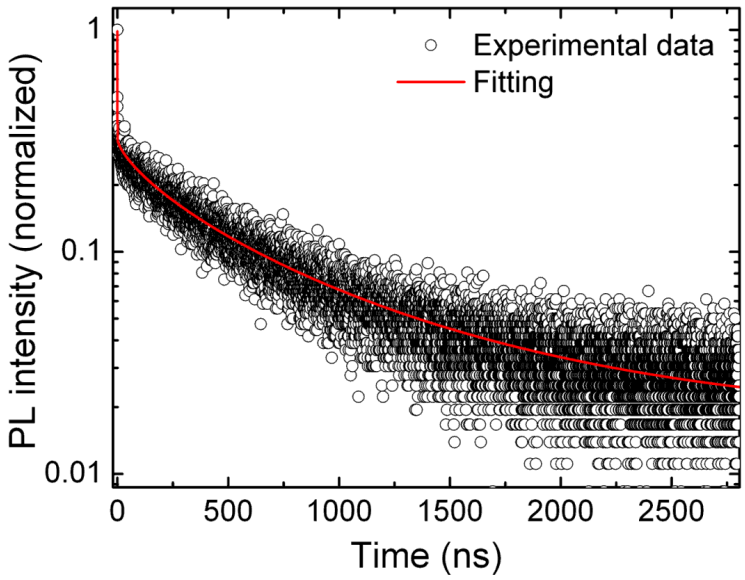

Figure S6 Time-resolved photoluminescence from $Cs_2AgBiBr_6$ single crystals. The excitation wavelength used was: 397.7nm, with a fluence of 46 nJ/cm^2.

The measurement in Figure S6 has been carried at room temperature with the same laser as described in the Experimental Section 6, but with a TCSPC detection scheme with a repetition rate of 300 Khz. The excitation wavelength is 397.7 nm, with a fluence of 46 nJ/cm^2.
We notice that the time-resolved photoluminescence kinetics is composed by two different processes: a fast decay and a long one. Fitting the data with the sum of a monoexponential decay (fast process) and a stretched exponetial decay (slower process) we get average lifetimes: $\tau_1 \sim 0.25$ ns for the fast decay, and $\tau_2 \sim 0.43$ µs for the long one.

5) Reflectivity measurements analysis

The reflectivity data collected are shown in Figure S7. Representative spectra were fitted to the real part of the linear susceptibility χ using the relation:

$$\sum_j A_j \frac{E_j^2 - E^2}{\gamma_j^2 + (E^2 - E_j^2)^2}$$

where A_j, E_j and γ_j are the amplitude, resonance energy and broadening parameter for any resonances present. In practice increased precision could be obtained using differential reflectivity as illustrated in Figure S8 where the real and imaginary parts of the dielectric function are plotted as a function of reduced frequency. These have been used to calculate the reflectivity of a thick crystal and the derivative reflectivity dR/dE. This demonstrates that the derivative plot shows a peak close to the original resonance with a FWHM of approximately half that of the original dielectric function.

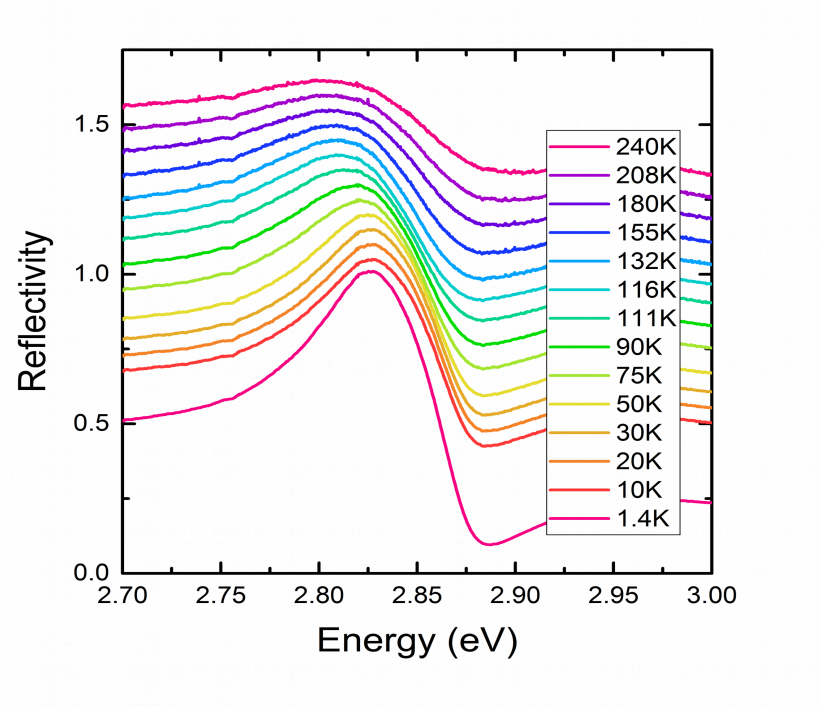

Figure S7 Experimental data for the temperature dependent reflectivity used for the derivative analysis shown in the main text.

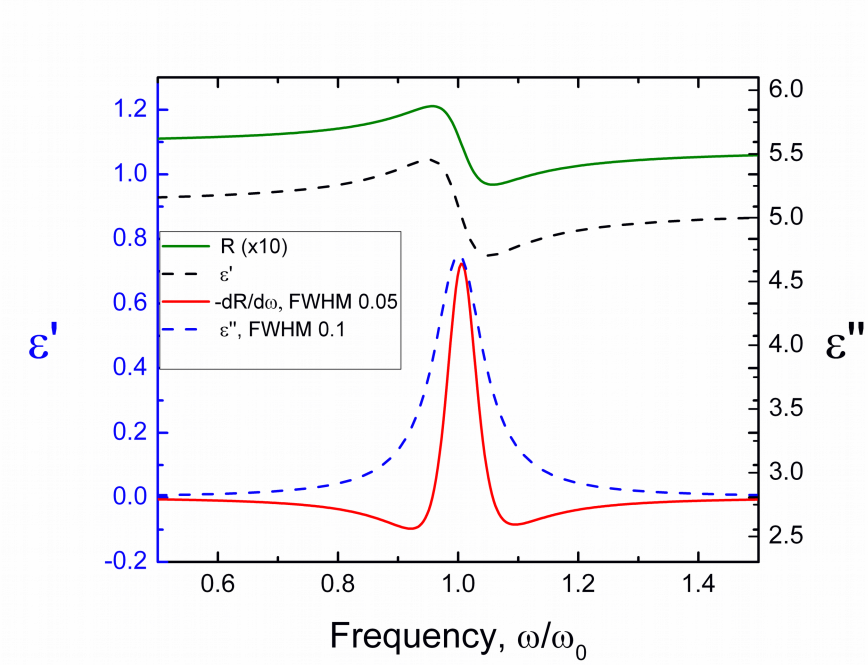

Figure S8 Modelled frequency (Energy) response of a typical absorption resonance showing the dependence of the real and imaginary components of the dielectric function, the reflectivity, R and its derivative.

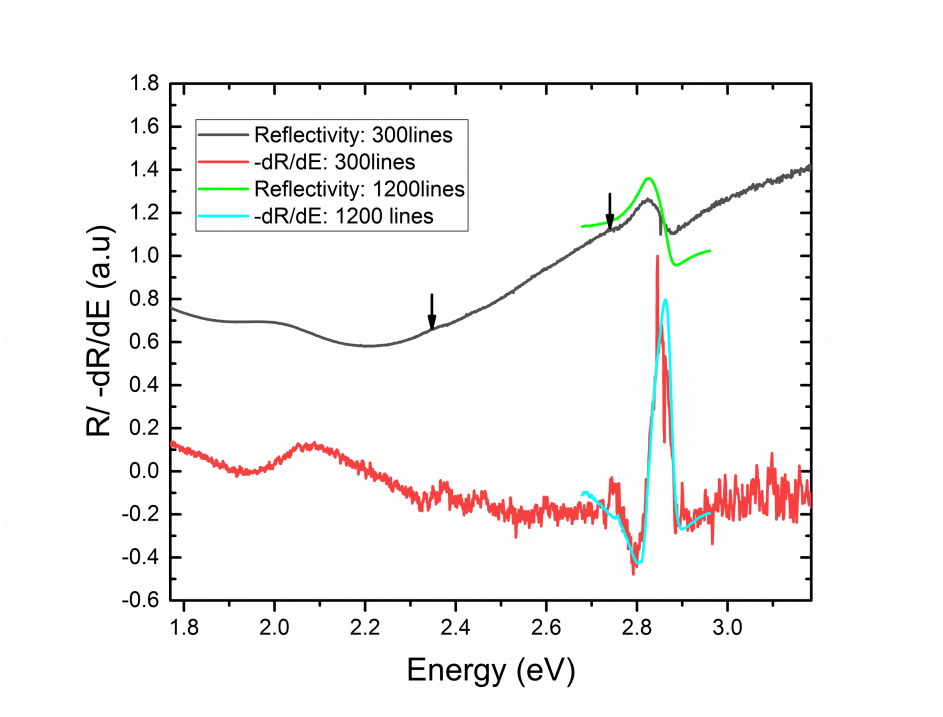

Figure S9 Overview of the reflectivity at 1.4K in the range of energies of interest for this study. The only –dR/dE peak is at ~2.86eV. As a comparison, the 1200 line grating used for the data shown in the main text, which allows for a higher resolution, is included here showing a good agreement. The black arrows indicate errors in the original data introduced by flaws in the 300 line grating used to obtain the continuous overview of the entire energy range of interest. For clarity, the data has been offset and scaled.

6) Experimental details

X-ray diffraction (XRD)

Single crystal X-ray diffraction has been performed using an Agilent Supernova diffractometer with Mo-Kα radiation. Powder X-ray diffraction has been performed using a PANalytical X'Pert PRO diffractometer with Cu -Kα radiation. The temperature change has been achieved employing an Oxford Cryosystems PheniX cryostat.

Neutron powder diffraction

Neutron powder diffraction has been performed using the time-of-flight diffractometer POLARIS (a high flux, medium resolution diffractometer) at the ISIS Spallation Neutron Source, UK. A ~5 g powder sample was loaded into a 6mm diameter cylindrical vanadium can. Room temperature data were collected for 350 μA.hours integrated proton beam current to the ISIS target, corresponding to ~2 hours beamtime. The sample was then removed from the sample changer and placed in a helium flow "orange" cryostat and cooled slowly from room temperature to 30K. The low temperature data set was collected for 450 μA.hours (corresponding to ~2.6 hours beamtime).

Heat capacity measurement

The heat capacity has been measured with the use of a Quantum Design Physical Properties Measurement System, varying the temperature of the sample (a 5.2 mg single crystal).

Reflection-transmission measurement

The sample was mounted in a gas-exchange helium cryostat (Oxford Instruments, OptistatCF2) and heated over temperatures from 5 to 295 K in increments of 5 K. To measure the reflectance and transmittance spectra, an FTIR spectrometer (Bruker Vertex 80v) was used, configured with a tungsten halogen lamp illumination source, a CaF2 beamsplitter and a silicon detector. (Data plotted in Figure 3 of the main text).

Time-resolved photoluminescence

The samples were photoexcited by a 398 nm picosecond pulsed diode laser (PicoHarp, LDH-D-C-405M). The resultant PL was collected and coupled into a grating spectrometer (Princeton Instruments, SP-2558), which directed the spectrally dispersed PL onto an iCCD (PI-MAX4, Princeton Instruments) or a photon-counting detector (PDM series from MPD), whose timing was controlled with a PicoHarp300 TCSPC event timer. The sample was mounted in a gas-exchange helium cryostat (Oxford Instruments, OptistatCF2).
For the temperature-dependent measurements, PL spectra and transients were taken as the sample was heated over temperatures from 4 to 295 K in increments of between 5 and 25 K. A laser intensity of 62 W cm-2 was used when obtaining the PL spectra, and a fluence of 210 nJ cm-2 for the PL transients.

Steady state Photoluminescence map

The steady state PL (Figure 4 in the main text) was collected in a custom setup using a LaserQuantum Ventus532 532nm laser. To prevent side modes and higher orders being coupled into the fibre, the laser was passed through a 532nm Edmond optics notch filter and additionally a KG3 and KG5 filter. After the filters, the laser was coupled into a fibre leading to the exchange gas liquid helium cryostat. In the sample holder the laser was focussed to a <1mm2 spot size, and impinged the sample orthogonally, in the Faraday geometry. The resulting PL response was collected by a fibre bundle, leading to a Princeton Applied Research Model 1235 triple grating 0.3m spectrograph coupled to an Andor iDus 416 (QE>45% between 400-1000nm). The spectra were captured using an 84.3ms exposure time and 400 accumulations, to prevent white noise and cosmic rays from influencing the highly sensitive detector.

Reflectivity measurement

The reflectivity measurements were performed in the same setup as the steady state 532nm excited PL measurements. Instead of the laser, an Ocean Optics HL-2000-FHSA halogen white light source was directly coupled into the fibre leading to the sample.
To account for the background in the signal caused by reflections caused by the setup and the fibre, all reflectivity measurements were divided by a reference measurement. This method effectively removed all noise and left the reflectivity signal coming from the sample unchanged.